

Seasonal and Long-Term Changes in the Intensity of $O_2(b^1\Sigma)$ and $OH(X^2\Pi)$ Airglow in the Mesopause Region

V. I. Perminov^{a, *}, N. N. Pertsev^{a, **}, P. A. Dalin^{b, c}, Yu. A. Zheleznov^d,
V. A. Sukhodoev^a, and M. D. Orekhov^a

^a *Obukhov Institute of Atmospheric Physics, Russian Academy of Sciences, Moscow, Russia*

^b *Swedish Institute of Space Physics, Kiruna, Sweden*

^c *Space Research Institute, Russian Academy of Sciences, Moscow, Russia*

^d *Institute of Electrophysics and Electric Power, Russian Academy of Sciences, St. Petersburg, Russia*

*e-mail: v.perminov@rambler.ru

**e-mail: n.pertsev@bk.ru

Received January 15, 2021; revised January 20, 2021; accepted January 28, 2021

Abstract—Spectral observations of the mesopause airglow at the Zvenigorod Scientific Station have been used to obtain the midnight emission intensities of molecular oxygen ($O_2A(0-1)$ band) and hydroxyl ($OH(6-2)$ band) for 2000–2019. Spectral analysis of the variations has made it possible to determine the annual variability for each emission, which is described by the sum of four harmonics. The time lag in seasonal variations of the hydroxyl emission relative to variations in the emission of molecular oxygen is 5–18 days. Long-term changes in the average annual emission intensities have been studied. The linear trend ($-3.3 \pm 0.3\%$ per year for $O_2A(0-1)$ and $-2.6 \pm 0.2\%$ per year for $OH(6-2)$), the dependences on the 11-year solar cycle (response to changes in the Lyman-alpha solar radiation ($18.5 \pm 3.3\%$ per 10^{11} photons $cm^{-2} s^{-1}$ for $O_2A(0-1)$ and $10.5 \pm 2.5\%$ per 10^{11} photons $cm^{-2} s^{-1}$ for $OH(6-2)$) and the 22-year solar cycle (response to changes in the solar magnetic field strength ($23.2 \pm 4.5\%$ per 100 μT for $O_2A(0-1)$ and $12.1 \pm 3.5\%$ per 100 μT for $OH(6-2)$), as well as quasi-eight-year oscillations have been found.

DOI: 10.1134/S0016793221040113

1. INTRODUCTION

The variations in the characteristics of the mesopause region (80–100 km) are currently addressed in many studies on the Earth's upper atmosphere. The changes can be caused by both heliogeophysical factors (solar electromagnetic and corpuscular radiation and dynamic processes in the atmosphere) and the effect of the anthropogenic impact on the environment. Observations of the airglow of atmospheric gases are one of the most efficient methods for the study of the mesopause region. Measurements of the intensity and spectral structure of the airglow bands make it possible to estimate the concentrations of the gas components and the temperature. Some studies indicate that the airglow characteristics of the mesopause are subjected to significant spatial and temporal variations. These variations include oscillations spanning from several minutes (normally of irregular character) to several decades. Long-term variations are the least studied of them, since the observation time series are limited. In addition, the latitudinal–longitudinal irregularities and specific features of the altitudinal distribution of emitting gases create local features of

seasonal (and smaller time-scale) changes in the characteristics of mesopause airglow.

The study is focused on two emissions related to the intrinsic radiation of the mesopause: the molecular oxygen ($A(0-1)$ band of the $O_2(b^1\Sigma)$ atmospheric system, 865 nm) and the hydroxyl ($(6-2)$ band of $OH(X^2\Pi)$, 835 nm). In the daytime, $O_2(b^1\Sigma)$ airglow occurs between 40 and 110 km due to the fluorescence, ionization, and chemical recombination reactions of atomic oxygen. However, only the latter are the key process for the formation of the emitting layer at night, which is localized between 85 and 105 km with a peak of ~ 94 km (Shefov et al., 2006). $OH(X^2\Pi)$ airglow, which also results from the chemical recombination of oxygen atoms, forms a layer in the range of 75–100 km with a maximum of ~ 87 km (Shefov et al., 2006).

The goal of the study is to determine the seasonal variation and long-term changes in the intensity of the aforementioned emission bands of molecular oxygen and hydroxyl in the mesopause. To this end, we analyzed the series of their long-term observations at the Zvenigorod Scientific Station ($56^\circ N$, $37^\circ E$) of the A.M. Obukhov Institute of Atmospheric Physics, Russian Academy of Sciences (Moscow).

Table 1. Amplitudes and phases of the harmonics of the annual course of O₂A(0-1) and OH(6-2) emission intensities

Harmonic	Emission of O ₂ A(0-1)		Emission of OH(6-2)	
	A_i , R	f_i , days	A_i , R	f_i , days
0	265.2 ± 3.3	—	710.7 ± 6.2	—
1	65.6 ± 4.6 (24.7 ± 1.7%)	302.4 ± 4.1	53.3 ± 9.8 (7.5 ± 1.4%)	321.8 ± 9.4
2	35.1 ± 4.4 (13.2 ± 1.7%)	31.8 ± 3.9	52.6 ± 9.2 (7.4 ± 1.3%)	17.2 ± 5.1
3	20.8 ± 4.6 (7.7 ± 1.7%)	40.5 ± 4.1	44.8 ± 9.4 (6.3 ± 1.3%)	52.3 ± 3.7
4	36.9 ± 4.2 (13.9 ± 1.6%)	76.4 ± 1.7	58.1 ± 8.5 (8.2 ± 1.2%)	85.8 ± 2.1

Hereafter, one standard deviation is indicated as an error of the parameter. The phases are given for the first maximum. The percentage values are indicated relative to the zero harmonic.

2. OBSERVATIONS

Spectral observations of the mesopause airglow in the near-infrared region (0.77–1.05 μm) were conducted at the Zvenigorod station with an SP-50 high-aperture spectrograph (Gerasimova and Yakovleva, 1956). The instrument is equipped with a recording camera with a high-sensitivity CCD-matrix cooled to –50°C. A detailed description of the equipment, observation technique, spectral processing, and the determination of the characteristics of molecular oxygen and hydroxyl emissions can be found in the literature (Pertsev and Perminov, 2008; Semenov et al., 2002; Shefov et al., 2006).

The observations are conducted on an ongoing basis in cloudless weather at a zenith angle of 53° in the northwestern direction (azimuth 23°, measured from north to west). The spectrum exposure time was 10 min. The observation conditions and the instrument specifications made it possible to determine the intensities of the O₂A(0-1) and OH(6-2) bands with a measurement error of 5–6 R (1 R = 10⁶ photons cm⁻² s⁻¹). The obtained emission intensities were reduced to the zenith conditions.

3. DATA ANALYSIS

This analysis considered the intensities (I) measured in 2000–2019. Each intensity series consists of 1663 values, the averages from 2100 to 2200 UT, i.e., around local midnight. This daily time interval made it possible to measure the emission intensities in both winter and summer, when only twilight conditions persisted at the observation latitude (56° N). Figure 1 shows these series. As can be seen, the emission intensities undergo significant changes over the entire long-term observation period, from three dozen to 1000 R for O₂A(0-1) and from 200 to 2000 R for OH(6-2). Among these changes, regular seasonal variations can be identified. Their spectrum was determined from LS-periodograms (Lomb, 1976; Scargle, 1982); see

Fig. 2. The first four harmonics are of high significance. Their normalized power (S_n) on the periodograms exceeds the level of statistical significance $\alpha = 0.05$. The harmonic characteristics were estimated with the multiple-regression method. The series of emission data were approximated with the expression

$$I = A_0 + \sum_{i=1}^4 A_i \cos\left(\frac{2\pi i}{365.25} (t - f_i)\right), \quad (1)$$

where A_0 is the zero harmonic; A_i and f_i are the amplitude and phase of the maximum of the i th harmonic; and t is the day number counted from January 1, 2000. The approximation results are presented in Table 1. The resulting A_0 values indicate that the average intensities of O₂A(0-1) and OH(6-2) for 2000–2019 are 265.2 ± 3.3 R and 710.7 ± 6.2 R, respectively. The amplitudes of the seasonal harmonics are from ~21 to ~66 R for the first emission and from ~45 to ~58 R for the second.

The interannual changes in emission intensities can be more clearly considered based on their average values for 1-year time intervals (I_{am}). Since the observational data for most years are unevenly distributed, a more accurate estimate of I_{am} values could be obtained if A_0 is determined from emission data approximated on the annual time interval with the sum of harmonics (1). For a better detailing of the interannual behavior of the emission intensity, the I_{am} values were determined for the time intervals from January 1 to December 31 and from July 1 of one year to June 30 of the following year. The resulting series are shown in Figs. 3a and 3c. One can see a significant decrease, which can be expressed linearly as

$$I_{\text{am}} = (376.0 \pm 16.7) - (10.7 \pm 1.5)(t - 2000) \quad (2)$$

for O₂A(0-1),

$$I_{\text{am}} = (920.2 \pm 27.2) - (21.4 \pm 2.5)(t - 2000) \quad (3)$$

for OH(6-2),

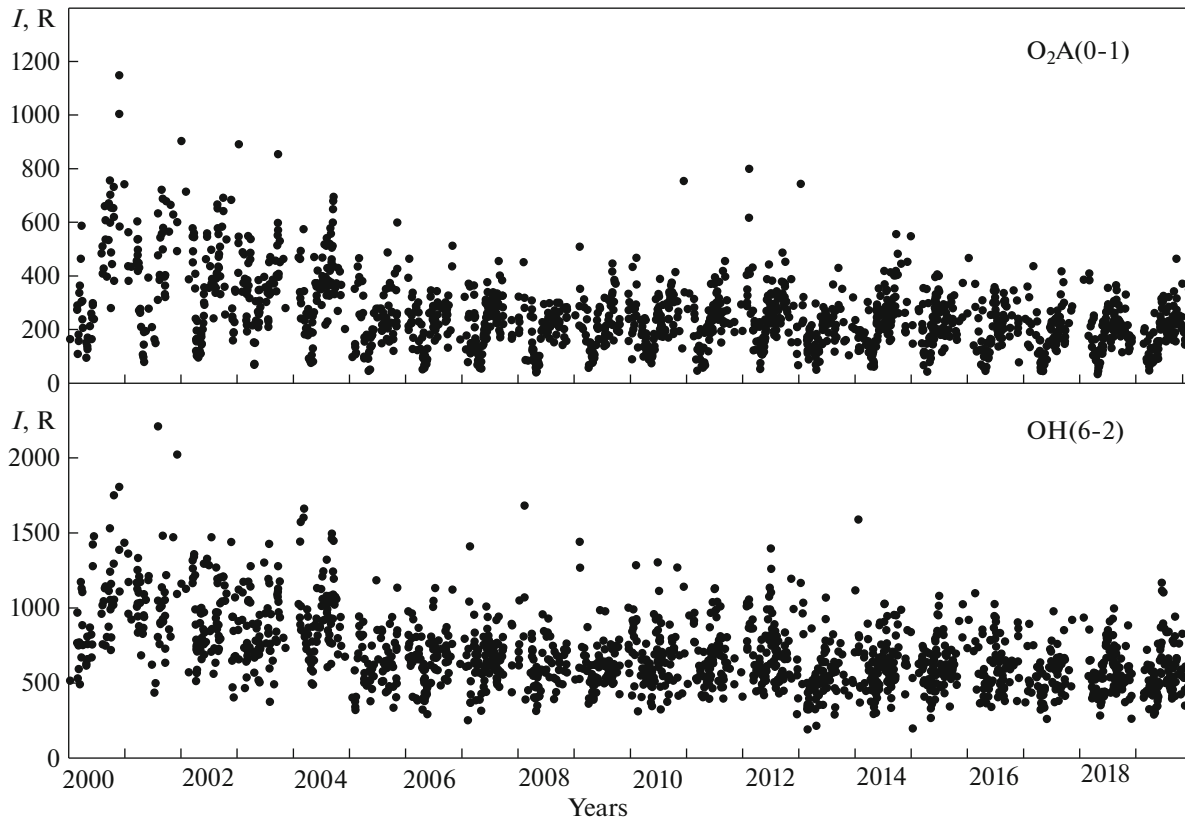


Fig. 1. Intensities (I) of $O_2A(0-1)$ (top) and $OH(6-2)$ (bottom) emissions according to observations at the Zvenigorod station in 2000–2019. The dots are averages for 21–22 UTC.

where t is the calendar year. The linear coefficient is measured in R/year . Expressions (2) and (3) were obtained with the least squares method. They are shown in Figs. 3a and 3c as straight solid lines. However, the calculated LS -periodograms of variations for these series show (Figs. 3b and 3d) that both the long-term changes (trend) and the 11-year oscillation, which is most likely associated with the 11-year solar activity cycle, are significant (Shefov et al., 2006). The region of periods of more than 20 years is shown on the periodograms by a dashed line, since the values of the periodic signal power here may be unreliable due to shorter data series as compared to the determined periods. The relationship between the emission intensities and solar activity was determined with the multiple-regression method:

$$I_{\text{am}} = (357.2 \pm 12.3) - (6.6 \pm 1.3)(t - 2000) + (73.5 \pm 11.8)(F_{L\alpha} - 4.5 \times 10^{11}) \text{ for } O_2A(0-1), \quad (4)$$

$$I_{\text{am}} = (893.0 \pm 21.7) - (15.4 \pm 2.2)(t - 2000) + (106.4 \pm 20.9)(F_{L\alpha} - 4.5 \times 10^{11}) \text{ for } OH(6-2), \quad (5)$$

where $F_{L\alpha}$ is the annual average Lyman-alpha (L_{α}) radiation flux in units of 10^{11} photons $\text{cm}^{-2} \text{s}^{-1}$, which was taken as an indicator of solar activity. The unit of the linear coefficient for coupling with $F_{L\alpha}$ is

$R/10^{11}$ photons $\text{cm}^{-2} \text{s}^{-1}$. The $F_{L\alpha}$ values are taken from the LASP Interactive Solar Irradiance Data Center (<https://lasp.colorado.edu/lisird>). Both emissions are characterized by lower values of the negative linear trend in comparison with the values in (2) and (3), as well as by a positive response to 11-year changes in solar activity. In the case of (4) and (5), the determination coefficient was ~ 0.8 , which shows a significant fraction of the revealed variations in the total variance of I_{am} values. However, the remaining fraction (~ 0.2) of the variance can also be associated with significant variations. Therefore, it made sense to study them in the series of residual intensities (ΔI_{am}) of emissions (Figs. 4a and 4c). ΔI_{am} is the difference between initial data series (Figs. 3a and 3c) and their approximations (4) and (5). Figures 4b and 4d show the LS -periodograms of the corresponding variations. It can be seen that the oscillation with periods of ~ 8 years is statistically significant for both emissions. The verification showed that the quasi-eight-year periodicity appears precisely in the residual intensities ΔI_{am} , rather than being a consequence of the subtraction of the solar-conditioned component in (4) and (5) from the initial I_{am} series. A significant peak of ~ 21 years is located near periods longer than the length of the analyzed series; therefore, it can only serve as a reference in the deter-

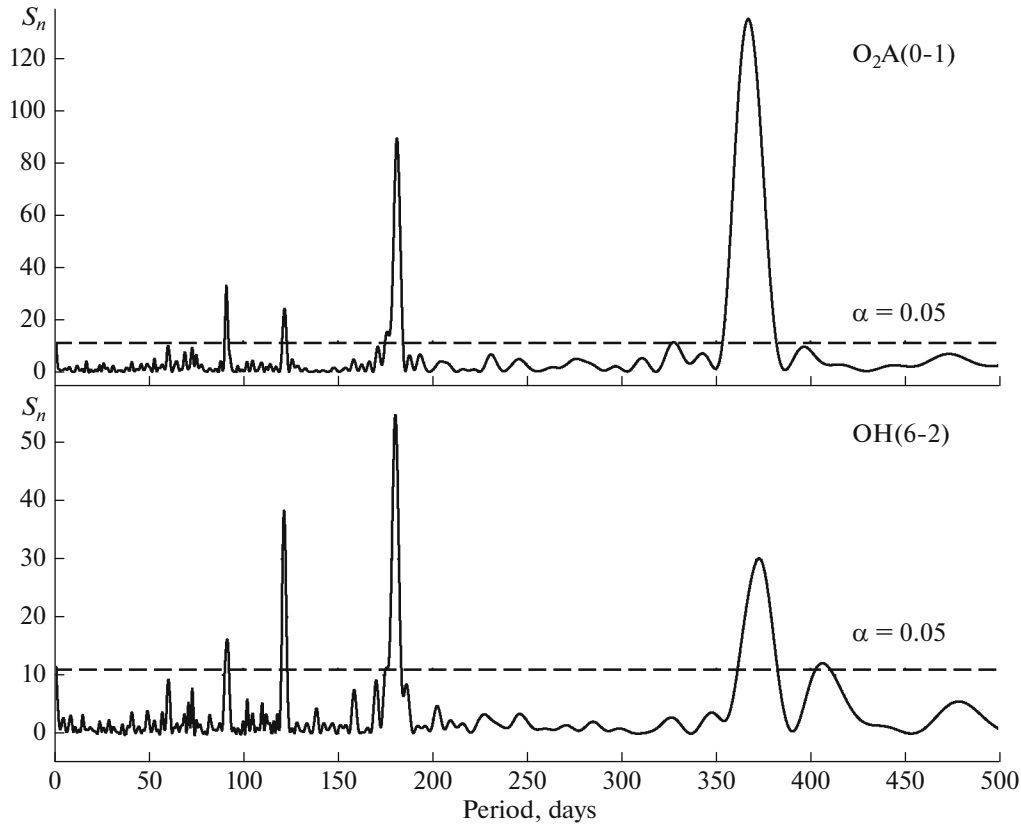


Fig. 2. LS-periodograms of emission intensity variations in the range of 1–500 days. S_n is the variation power normalized to the variance of intensity I . The dashed line is the level of statistical significance (α).

mination of a possible physical basis for the relationship between the emission intensity and atmospheric processes of the proposed periodicity. Höppner and Bittner (2007) and Kalicinsky et al. (2016) linked the long-term changes in the characteristics of the thermodynamic regime of the mesopause region with the 22-year cyclicality of changes in the solar magnetic field (the Hale cycle). In Figure 5, one can visually compare the interannual changes in ΔI_{am} with the corresponding changes in the solar magnetic field. The average strength (B) of the magnetic field at latitudes above 55° N and S was taken as an indicator of the solar magnetic field. The values of B are taken in microteslas (μT) according to observations at the Wilcox Solar Observatory of Stanford University (<http://wso.stanford.edu/Polar.html>). It can be seen that the comparison should take into account the time lag between changes in the solar magnetic field and mesopause emissions.

The parameters of all emission-intensity relationships were estimated via multiple regression with the approximation of series I_{am} as

$$I_{am} = A_0 + A_{tr}(t - 2000) + A_{L\alpha}(F_{L\alpha} - 4.5 \times 10^{11}) + A_{MFS} \frac{B_{(t-\Delta t)}}{100} + A_{QOO} \cos\left(\frac{2\pi}{T_{QOO}}(t - f_{QOO})\right), \quad (6)$$

where A_0 is a constant; A_{tr} is the linear trend coefficient (R/year); $A_{L\alpha}$ is the response of emissions to changes in the flux $F_{L\alpha}$ (R/ 10^{11} photons $\text{cm}^{-2} \text{s}^{-1}$); $B_{(t-\Delta t)}$ is the annual average value of the strength of the polar magnetic field of the Sun for the year corresponding to $t - \Delta t$ (Δt is the time lag between changes in the solar magnetic field and the intensity of emissions at the mesopause); A_{MFS} is the response of emissions to changes in the strength of the polar magnetic field of the Sun (R/ μT); and T_{QOO} , A_{QOO} , and f_{QOO} are the period, amplitude, and phase of the maximum of the quasi-eight-year oscillation (QOO). Table 2 gives the resulting estimates for the parameters of the regression model (6). The best correlation between its dependent variables is found at a lag of 2.5 years. A positive lag shows that the variations in the emission intensity lag behind the variations in the solar magnetic field. Regression analysis allowed the quasi-eight-year oscillation period to be refined from the condition of the highest multiple correlation coefficient. This period was 7.7 years for $\text{O}_2\text{A}(0-1)$ and 8.2 years for $\text{OH}(6-2)$. In view of the coefficient of determination (see R^2 in Table 2), more than 92% of the variance of intensity I_{am} in 2000–2019 was due to the constraints and variations taken into account in (6).

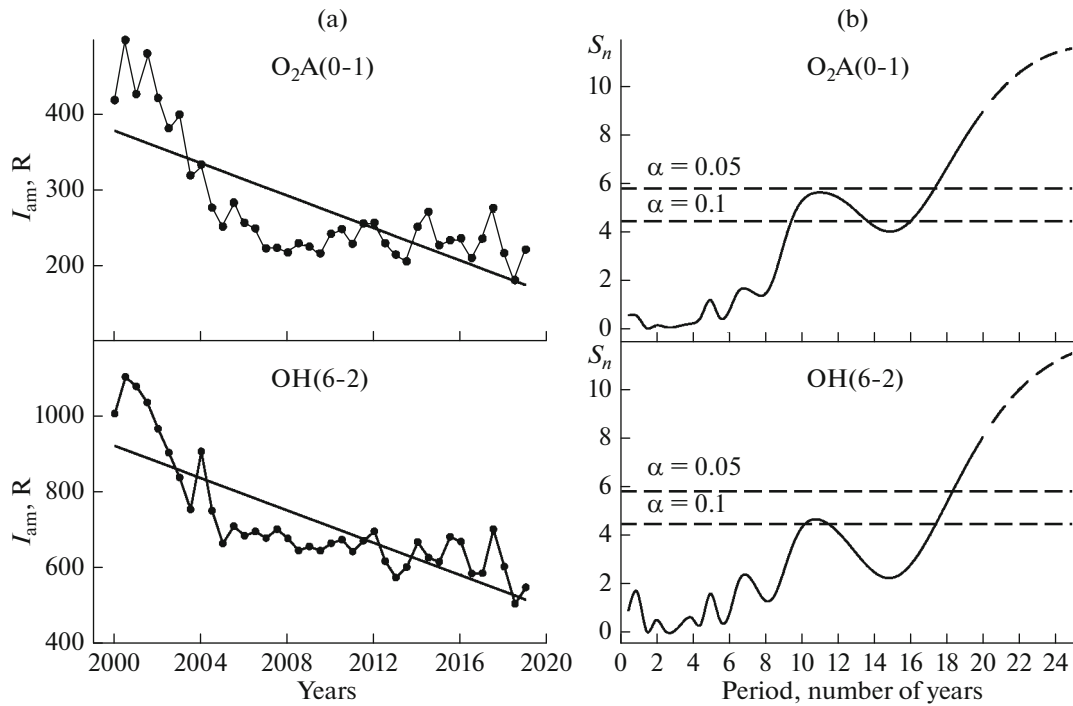


Fig. 3. (a) Long-term changes in the intensity (I_{am}) of emissions. The dots show the annual averages. The solid line is the trend according to expressions (2) and (3). (b) *LS*-periodograms of variations. S_n is the variation power normalized to the variance of I_{am} values. The domain of S_n values in the range of periods of 20–25 years is shown by the dashed curve line, since the values of the periodic signal power may be unreliable due to the shorter length of the data series as compared to the determined periods. The dashed straight lines show the levels of statistical significance (α).

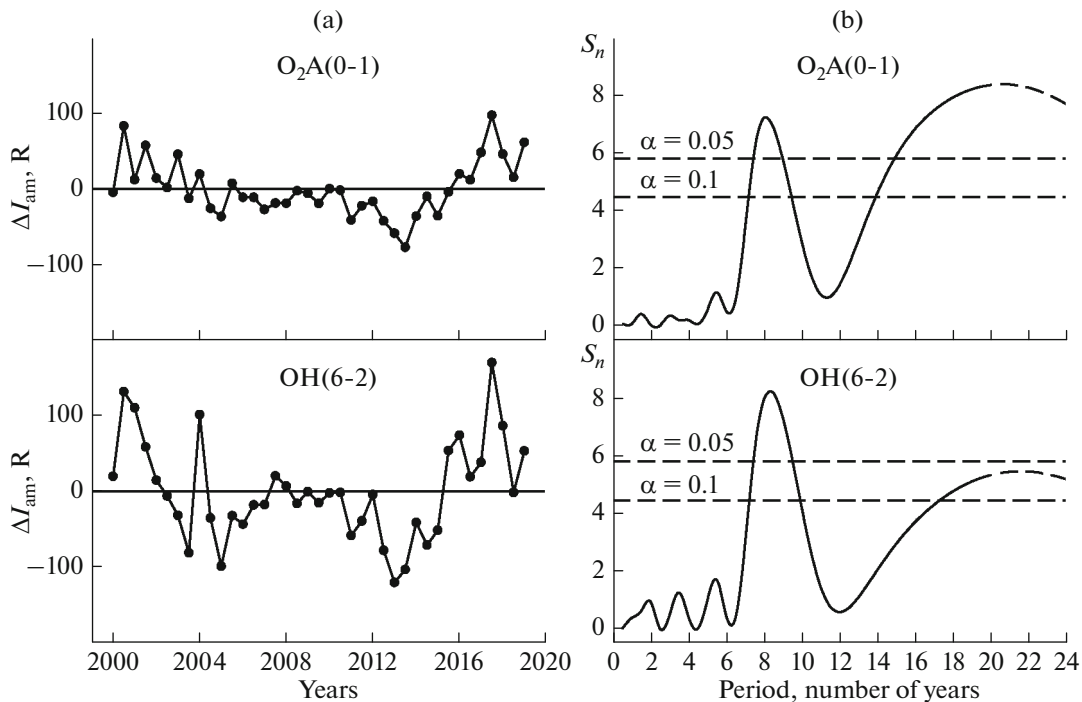


Fig. 4. (a) Interannual variations in the residual emission intensity (ΔI_{am}). (b) *LS*-periodograms of variations. The notations are the same as in Fig. 3.

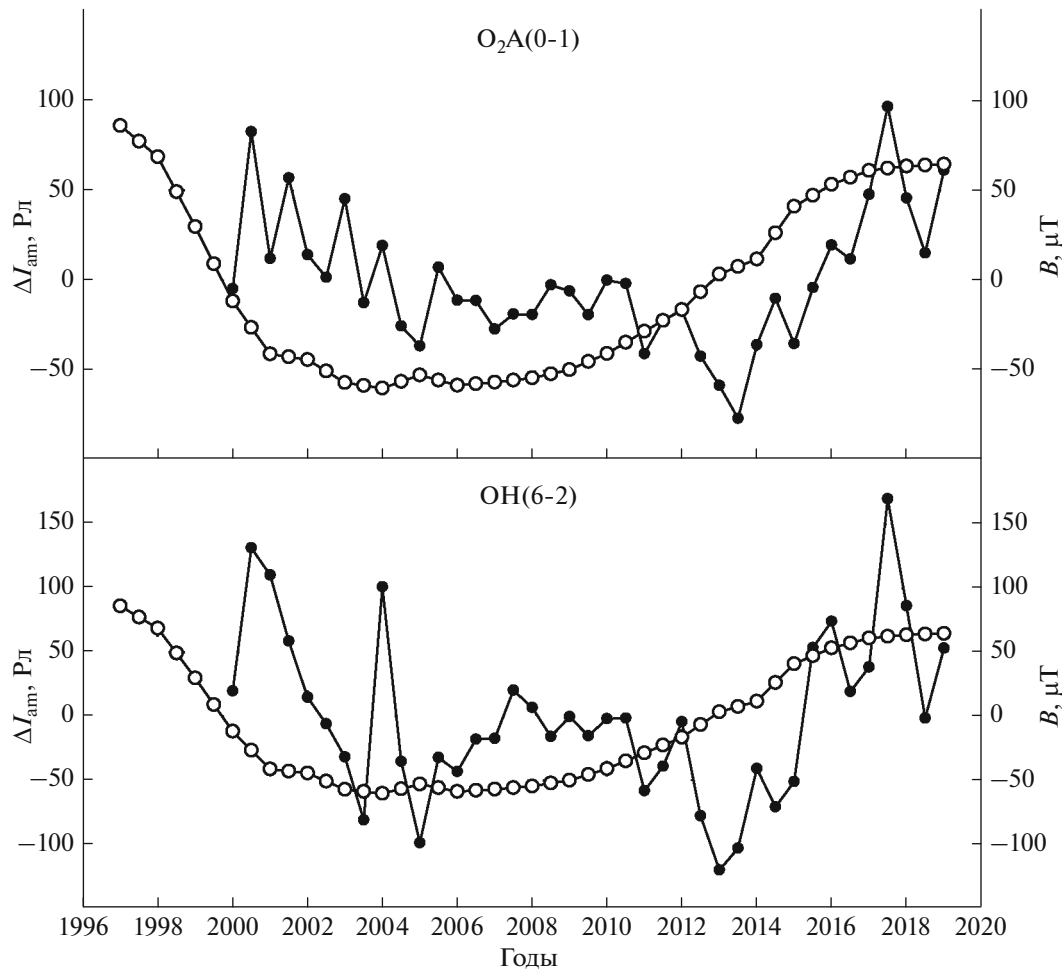


Fig. 5. Interannual changes in the residual intensity (ΔI_{am}) of $\text{O}_2\text{A}(0-1)$ (top) and $\text{OH}(6-2)$ (bottom) emissions and the solar magnetic field. Dark circles show the values of emission intensity. Light circles show the average annual values of strength (B) of the polar magnetic field of the Sun.

4. DISCUSSION

4.1. Seasonal Variations

According to Fig. 1, the emission intensity can vary significantly between nights. However, a certain regular course is retained within each year; it can be represented as a superposition of four relative harmonics as in Fig. 6a (the graphs were obtained from data of Table 1). It can be seen that both emissions are not only similar but also have some specific features that can be described as follows.

(1) The emissions have a similar, four-peak seasonal pattern. However, the variations in intensity of $\text{O}_2\text{A}(0-1)$ are ahead of the corresponding variations in the intensity of $\text{OH}(6-2)$ by 5–18 days.

(2) The highest relative seasonal variations are observed in the intensity of $\text{O}_2\text{A}(0-1)$. The amplitudes of its harmonics are 8–25% of the annual average intensity. During the spring minimum (late April–early May), its values decrease to 40% of the annual average. The highest values are found in the vicinity of the fall equinox (exceeding the annual average by 35%). The amplitudes of the harmonics of seasonal

Table 2. Estimated parameters of multiple regression (6)

Emissions	A_0 , R	A_{tr} , R/year	$A_{L\alpha}$, R/ 10^{11} photon $\text{cm}^{-2} \text{s}^{-1}$	A_{MFS} , R/100 μT	A_{QOO} , R	F_{QOO} , year	R^2
$\text{O}_2\text{A}(0-1)$	378.3 ± 9.0	-8.7 ± 0.9	49.1 ± 8.8	61.5 ± 11.8	17.7 ± 5.9	2002.3 ± 0.4	0.93
$\text{OH}(6-2)$	921.0 ± 17.8	-18.2 ± 1.7	75.0 ± 18.0	85.7 ± 25.1	33.3 ± 12.9	2000.8 ± 0.4	0.92

R^2 is the square of multiple correlation (determination coefficient).

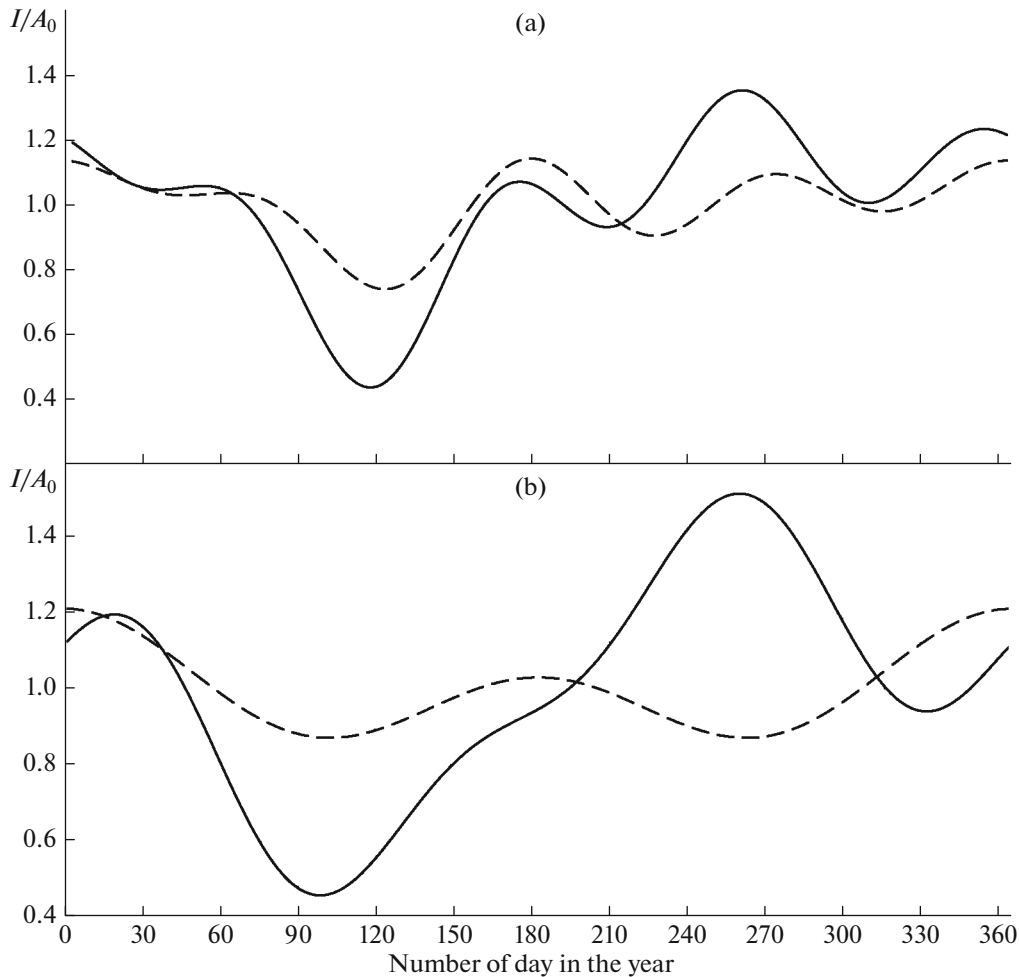


Fig. 6. Seasonal variation of the intensity of $O_2A(0-1)$ (solid line) and $OH(6-2)$ (dashed line) emissions: (a) according to Table 1; (b) according to (Shefov et al., 2006) for the latitude $56^\circ N$. The intensity values are taken as their ratio to the zero harmonic A_0 .

variations in $OH(6-2)$ are more weakly expressed: 6–8% of the average intensity.

There are a sufficiently large number of experimental studies of seasonal variations in the emissions of molecular oxygen and hydroxyl (Fishkova, 1983; Perminov and Pertsev, 2010; Pertsev and Perminov, 2008; Teiser and von Savigny, 2017; Wiens and Weill, 1973; Gao et al., 2010; Liu et al., 2008; Lopez-Gonzalez et al., 2004; Perminov et al., 2007; Reid et al., 2014; Scheer et al., 2005; Shefov et al., 2006). Shefov et al. (2006) analyzed observations up to the mid-2000s to determine the parameters of the first three seasonal harmonics of O_2 airglow and two harmonics of OH airglow. It was also established that the harmonics of the first emission depend on the latitude. Figure 6b shows the seasonal variation of emission intensities for latitude $56^\circ N$ according to Shefov et al. (2006). It can be seen in this case that the variations of both emissions are not as similar as in our study; therefore, one cannot speak about any delay between them.

Attention should be drawn to the results of studies by Lopez-Gonzalez et al. (2004) and Scheer et al. (2005). They describe seasonal changes in the present emissions for latitudes $37^\circ N$ and $32^\circ S$, which were obtained via averaging of the data with a 1-month window. At each latitude, the emission intensities have a similar annual course with a 1- to 1.5-month lag in hydroxyl-emission variations. Obviously, the delay in this case cannot be estimated more accurately, because the measurements were strongly smoothed.

The features of the annual variation of hydroxyl airglow with latitude (from $50^\circ S$ to $50^\circ N$) are shown based on global measurements with the TIMED radiometer from the SABER satellite (Gao et al., 2010). This study gives evidence of the dominance of the semiannual harmonic at the equator and a gradual increase in the annual harmonic with increasing latitude. Gao et al. (2010) did not find the fourth harmonic of the annual course (only the first three harmonics were found); however, Teiser and von Savigny (2017) used data from other satellite observations of

hydroxyl emission (SCIAMACHY/Envisat) to find the fourth and fifth harmonics in the spectrum of seasonal variations at low latitudes. However, Teiser and von Savigny (2017) did not analyze these harmonics; they used them only to improve the estimates of annual and semiannual oscillations. In this study, the annual course of the hydroxyl-emission intensity is more complex: it is described by four equivalent harmonics (without dominance of the first harmonic).

Perminov and Pertsev (2010) showed that the seasonal variations in the intensity of the present emissions are a reflection of combined seasonal variations in the temperature and the concentrations of the main atmospheric gases (O_2 and N_2) and atomic oxygen; here, positive changes in the concentrations of the gaseous components cause an increase in the emission intensity, and the corresponding changes in temperature cause a decrease (due to the slowing of chemical reactions, which leads to the excitation of oxygen and hydroxyl molecules). A number of studies suggest a decisive role in the seasonal behavior of mesopause emissions to temperature changes and the dynamics of atomic oxygen, or they emphasize the role of only the latter process (Grygalashvyly et al., 2014, 2015; Liu et al., 2008; Sonnemann et al., 2015).

4.2. Long-Term Changes

4.2.1. Trend

Our analysis revealed a negative linear trend in emission intensity in 2000–2019. Due to all of the long-term processes in the mesopause region, its values are -10.7 ± 1.5 R/year ($-4.0 \pm 0.6\%$ per year) for $O_2A(0-1)$ and -21.4 ± 2.5 R/year ($-3.0 \pm 0.4\%$ per year) for $OH(6-2)$. When the effect of long-term solar activity cycles and quasi-eight-year oscillations are taken into account, the trend values decrease to -8.7 ± 0.9 R/year ($-3.3 \pm 0.3\%$ per year) for $O_2A(0-1)$ and -18.2 ± 1.7 R/year ($-2.6 \pm 0.2\%$ per year) for $OH(6-2)$. The percentage values are taken relative to the average intensities for the entire observation period (which corresponds to A_0 in Table 1). This is in good agreement with the previous recent study of long-term observations at the Zvenigorod station, which analyzed the trends in the emission intensity with allowance for the seasons of the year for 2000–2018 (Dalin et al., 2020).

The number of studies of the long-term trend is extremely small, and most of them analyze the intensity of hydroxyl emissions (Fishkova, 1983; Dalin et al., 2020; Shefov et al., 2006; Sonnemann et al., 2015; Teiser and von Savigny, 2017). The earliest and longest observations (1948–1980) of hydroxyl emission were conducted by Fishkova (1983). Analysis of these data, as well as the measurements at the Zvenigorod station and in Haute Provence in the 1950s–1960s (Shefov, 1969; Wiens and Weill, 1973), allowed Shefov et al. (2006) to conclude that there was a nonlinear increase

in the intensity of hydroxyl emissions at midlatitudes up to the 1980s. As a result, the total intensity of all hydroxyl-emission bands increased by $\sim 80\%$ (from ~ 550 kR (1948) to ~ 1 MR (1980)). Modern data for 2000–2019 indicate that the long-term course of hydroxyl emission now involves a phase of intensity decrease. It can be noted here that the rate of decline in magnitude is the same as that observed during the growth in the 1950s.

Sonnemann et al. (2015) used long-term monitoring of anthropogenic greenhouse gases (1961–2009) and their application in the LIMA model to calculate the interannual changes and the trend in the concentration of vibrationally excited hydroxyl (OH^*) in the region of its maximum airglow. At the midlatitudes, the model showed a small positive linear trend over the entire time interval (1961–2009). However, the interannual changes in 2000–2009 tend to decrease the OH^* concentration, which is consistent with the results of this study. Also, a negative trend in changes in the hydroxyl-emission intensity for the midlatitudes was obtained by Teiser and von Savigny (2017) based on the SCIAMACHY/Envisat satellite observations in 2002–2012.

Sonnemann et al. (2015) showed that the trend is largely caused by changes in the activity of planetary waves, tides, and internal gravity waves, rather than by long-term changes in the content of atmospheric greenhouse gases. Most likely, changes in the dynamics in the mesosphere and lower thermosphere are responsible for significant changes in the content of atomic oxygen in the emitting layers of hydroxyl and molecular oxygen.

4.2.2. Link to the 11-year solar cycle

The response of emissions to changes in the solar-radiation flux in the Lyman-alpha line, which is taken as an indicator of solar activity, is positive during the 11-year cycle and, by magnitude, is one of the most substantial of interannual variations. Its values are 49.1 ± 8.8 R/ 10^{11} photons $cm^{-2} s^{-1}$ ($18.5 \pm 3.3\%$ per 10^{11} photons $cm^{-2} s^{-1}$) for $O_2A(0-1)$ and 75.0 ± 18.0 R/ 10^{11} photons $cm^{-2} s^{-1}$ ($10.5 \pm 2.5\%$ per 10^{11} photons $cm^{-2} s^{-1}$) for $OH(6-2)$.

Earlier, Pertsev and Perminov (2008) and Dalin et al. (2020) analyzed data from emission observations at the Zvenigorod scientific station. The response of emissions to changes in the flux of solar radio emission (10.7 cm) recalculated into units of response to Lyman-alpha radiation (Pertsev and Perminov, 2008) gives overestimated values in comparison with real values by 1.4–1.7 times (68.1 ± 12.4 R/ 10^{11} photons $cm^{-2} s^{-1}$ for $O_2A(0-1)$ and 130.0 ± 19.6 R/ 10^{11} photons $cm^{-2} s^{-1}$ for $OH(6-2)$); however, they are in good agreement with the response values according to regressions (4) and (5). The response shown by Dalin et al. (2020) was specified separately for winter and summer. Their average values

(67.5 R/10¹¹ photons cm⁻² s⁻¹ for O₂A(0-1) and 103.5 R/10¹¹ photons cm⁻² s⁻¹ for OH(6-2)) are also quite consistent with the response values obtained in expressions (4) and (5).

One of the most detailed studies of the response of emissions from the mesopause region to changes in solar activity was performed by Gao et al. (2016). Based on the TIMED/SABER satellite data for hydroxyl emission, these authors showed the dependence of the solar response on latitude with a strong hemispheric asymmetry; the response peaks in the southern hemisphere. Both hemispheres are characterized by the fact that the greatest response values are observed at the boundaries of the given latitudinal zone: 50° S (10–11% per 10¹¹ L α -photons cm⁻² s⁻¹) and 50° N (8–9% per 10¹¹ L α -photons cm⁻² s⁻¹). The indicated response values result from the recalculation of the linear regression coefficients for the dependence on solar radio emission (10.7 cm). The response of hydroxyl emission to solar activity obtained in our study (10.5% per 10¹¹ photons cm⁻² s⁻¹) indicates that it further slightly increases with increasing latitude. However, this increase seems to differ by season and may have the opposite sign. Indeed, some studies using the LIMA model for low, middle, and high latitudes showed a decrease in the solar response of hydroxyl emission with increasing latitude for winter conditions and an increase for spring and summer conditions (Sonnemann et al., 2015). In this case, at a latitude of ~51° N, the response is predicted to be maximal for summer and minimal for winter. This could be explained by the fact that the change in the emission intensity is largely caused by the change in the content of atomic oxygen in the mesopause region. The summer conditions are favorable for the formation of oxygen atoms due to the longer photolysis of molecular oxygen under the influence of solar UV radiation. However, the results obtained by Sonnemann et al. (2015) contradict the observations at the Zvenigorod station; this means that the winter response exceeds the summer value by 40% (Dalin et al., 2020). Most likely, the primary reason for the seasonality of the solar response of mesopause emissions is possibly associated with changes in the processes controlling the atmospheric dynamics (which, in turn, are associated with the level of solar activity) rather than with the direct effect of solar UV radiation. Thus, studies of the long-term course of the activity of waves of various time and spatial scales are important (Perminov et al., 2014a, 2014b; Popov et al., 2020; Reisin et al., 2014).

4.2.3. Dependence on the solar magnetic field

In this study, we obtained not only the response of the emissions of the mesopause region airglow to the 11-year solar-activity cycle but also its dependence on the solar magnetic field, which has a 22-year periodicity (the Hale cycle). The solar magnetic field was char-

acterized by its power characteristic—the strength of the polar magnetic field. The coefficients of this linear dependence are 61.5 ± 11.8 R/100 μ T ($23.2 \pm 4.5\%$ per 100 μ T) for O₂A(0-1) and 85.7 ± 25.1 R/100 μ T ($12.1 \pm 3.5\%$ per 100 μ T) for OH(6-2). Here, these coefficients become statistically significant only when the changes in the intensity of mesopause emissions lag changes in the solar magnetic field by 2.5 years. It should be noted that the dependence of the solar magnetic field used in the regression model (6) significantly refines the emission response to changes in the Lyman-alpha radiation. This makes it difficult to compare the results obtained here and earlier in other studies, which tended to consider only the dependence on the 11-year cycle of solar activity.

Earlier, the dependence of the characteristics of the mesopause region on the level of the solar magnetic field was considered by Höppner and Bittner (2007) and Kalicinsky et al. (2016). Höppner and Bittner (2007) analyzed the planetary wave activity in the temperature of hydroxyl emission in Wuppertal (Germany) according to spectral observations in 1981–2005. As a result, there was good agreement with long-term changes in the solar magnetic field. Later, Kalicinsky et al. (2016) analyzed a longer series of the same temperature measurement data for Wuppertal to show that the long-term temperature trend in the mesopause region evolved, which may be due to the 22-year cyclicity of the solar magnetic field. Höppner and Bittner (2007) proposed a possible mechanism of the influence of the solar magnetic field on the mesopause region via its influence on the Earth's rotation. However, this mechanism requires experimental verification and model validation.

4.2.4. Quasi-eight-year oscillation

The amplitude of the revealed quasi-eight-year oscillation is 17.7 ± 5.9 R ($6.7 \pm 2.2\%$) for O₂A(0-1) and 33.3 ± 12.9 R ($4.7 \pm 1.8\%$) for OH(6-2). A similar variation was noted by Reid et al. (2014), who analyzed 15-year observations of the emission intensity of atomic oxygen (557.7 nm) and hydroxyl (OH(8-3) band, 730 nm) near Adelaide (Australia). A statistically significant oscillation with a period of ~3000 days (~8.2 years) was found on the spectra of hydroxyl-emission variations. This oscillation was not identified on similar spectra for the emission of atomic oxygen. This was apparently due to the powerful signal caused by the emission response to the 11-year oscillation in solar activity. Reid et al. (2014) found no physical basis for the oscillation with that period in the mesopause region and performed no analysis. However, variations with periods close to 8 years were identified in various climatic data associated with observations of temperature and pressure near the Earth's surface. Specifically, Plaut et al. (1995) analyzed a 335-year temperature series for central England to identify oscillations with a period of 7–8 years. Later, variations with a

similar period were identified in various climatic data for the regions of Europe, the North Atlantic and the Mediterranean (Paluš and Novotna, 1998, 2004; Feliks et al., 2010; Gamiz-Fortis et al., 2002; Kondrashov et al., 2005). Jajcay et al. (2016) recently showed that oscillations with a period of 7–8 years can have a modulating effect on the amplitudes of higher-frequency variations. This effect on tides may have been responsible for the 8-year oscillations of the emission intensity of the upper atmosphere observed in this study.

5. CONCLUSIONS

Spectral observations of the intrinsic radiation of the mesopause region at the Zvenigorod Scientific Station were used to obtain the intensities of the O₂A(0-1) and OH(6-2) bands for midnight conditions in 2000–2019. We can conclude the following.

(1) The seasonal variability of emissions is characterized by the sum of four harmonics; their amplitudes are the largest for the emission of molecular oxygen. The variations in the intensity of molecular-oxygen emission are 5–18 days ahead of the corresponding variations in the intensity of hydroxyl emission. The amplitudes of the harmonics are 8–25% for O₂A(0-1) and 6–8% for OH(6-2) of the average values of emission intensity for the observed time period.

(2) The linear trend of the emission intensity for 2000–2019 has negative values and is $-3.3 \pm 0.3\%$ per year for molecular oxygen and $-2.6 \pm 0.2\%$ per year for hydroxyl, which is indicative of opposite processes in the dynamics and energetics in the mesopause region as compared to 1948–1980, when a positive hydroxyl emission trend was observed.

(3) Along with the association with the 11-year cycle of solar activity (the indicator is the solar radiation flux in the Lyman-alpha line), the mesopause emissions depend on the solar polar magnetic strength (22-year cycle of the solar magnetic field reversal). In the first case, the response is $18.5 \pm 3.3\%$ for 10^{11} L α -photons cm⁻² s⁻¹ for O₂A(0-1) and $10.5 \pm 2.5\%$ for 10^{11} L α -photons cm⁻² s⁻¹ for OH(6-2). In the second case, the response values are $23.2 \pm 4.5\%$ per 100 μ T and $12.1 \pm 3.5\%$ per 100 μ T, respectively.

(4) The intensities of the mesopause emissions undergo statistically significant oscillations with periods of ~8 years. Their amplitudes are $6.7 \pm 2.2\%$ for O₂A(0-1) and $4.7 \pm 1.8\%$ for OH(6-2). These oscillations in the mesopause region may be associated with corresponding climatic oscillations in the state of the atmospheric surface layer.

FUNDING

This study was supported by the Russian Foundation for Basic Research, project no. 19-05-00358a.

CONFLICT OF INTERESTS

The authors state that there is no conflict of interests.

REFERENCES

- Dalin, P., Perminov, V., Pertsev, N., and Romejko, V., Updated long-term trends in mesopause temperature, airglow emissions, and noctilucent clouds, *J. Geophys. Res.: Atmos.*, 2020, vol. 125, e2019JD030814. <https://doi.org/10.1029/2019JD030814>
- Feliks, Y., Ghil, M., and Robertson, A.W., Oscillatory climate modes in the Eastern Mediterranean and their synchronization with the North Atlantic Oscillation, *J. Clim.*, 2010, vol. 23, no. 15, pp. 4060–4079.
- Fishkova, L.M., *Nochnoe izluchenie sredneshirotnoi verkhnei atmosfery Zemli* (Night Airglow of the Earth's Midlatitude Upper Atmosphere), Tbilisi: Metsniereba, 1983.
- Gamiz-Fortis, S., Pozo-Vazquez, D., Esteban-Parra, M., and Castro-Diez, Y., Spectral characteristics and predictability of the NAO assessed through singular spectral analysis, *J. Geophys. Res.*, 2002, vol. 107. <https://doi.org/10.1029/2001JD001436>
- Gao, H., Xu, J., and Wu, Q., Seasonal and QBO variations in the oh nightglow emission observed by TIMED/SABER, *J. Geophys. Res.*, 2010, vol. 115, A06313. <https://doi.org/10.1029/2009JA014641>
- Gao, H., Xu, J., and Chen, G.-M., The responses of the nightglow emissions observed by the TIMED/SABER satellite to solar radiation, *J. Geophys. Res.: Space*, 2016, vol. 121, pp. 1627–1642.
- Gerasimova, N.G. and Yakovleva, A.V., A system of high-transmission spectrographs with diffraction grating, *Prib. Tekh. Eksp.*, 1956, no. 1, pp. 86–95.
- Grygalashvily, M., Several notes on the OH* layer, *Ann. Geophys.*, 2015, vol. 33, no. 7, pp. 923–930. <https://doi.org/10.5194/angeo-33-923-2015>
- Grygalashvily, M., Sonnemann, G.R., Lübken, F.-J., Hartogh, P., and Berger, U., Hydroxyl layer: Mean state and trends at midlatitudes, *J. Geophys. Res.: Atmos.*, 2014, vol. 119, pp. 12391–12419.
- Höppner, K. and Bittner, M., Evidence for solar signals in the mesopause temperature variability?, *J. Atmos. Sol.-Terr. Phys.*, 2007, vol. 69, pp. 431–448.
- Jajcay, N., Hlinka, J., Kravtsov, S., Tsonus, A.A., and Paluš, M., Time scales of the European surface air temperature variability: The role of the 7–8 year cycle, *Geophys. Res. Lett.*, 2016, vol. 43, pp. 902–909.
- Kalicinsky, C., Knieling, P., Koppmann, R., Offermann, D., Steinbrecht, W., and Wintel, J., Long-term dynamics of OH* temperatures over central Europe: Trends and solar correlations, *Atmos. Chem. Phys.*, 2016, vol. 16, pp. 15033–15047.
- Kondrashov, D., Feliks, Y., and Ghil, M., Oscillatory modes of extended Nile River records (A.D. 622–1922), *Geophys. Res. Lett.*, 2005, vol. 32, L10702. <https://doi.org/10.1029/2004GL022156>
- Liu, G., Shepherd, G.G., and Roble, R.G., Seasonal variations of the nighttime O(1S) and OH airglow emission rates at mid-to-high latitudes in the context of the large-

- scale circulation, *J. Geophys. Res.*, 2008, vol. 113, A06302. <https://doi.org/10.1029/2007JA012854>
- Lomb, N.R., Least-squares frequency analysis of unequally spaced data, *Astrophys. Space Sci.*, 1976, vol. 39, no. 2, pp. 447–462.
- Lopez-Gonzalez, M.J., Rodriguez, E., Wiens, R.H., et al., Seasonal variations of O₂ atmospheric and OH(6-2) airglow and temperature at mid-latitudes from SATI observations, *Ann. Geophys.*, 2004, vol. 22, no. 3, pp. 819–828.
- Paluš, M. and Novotna, D., Detecting modes with nontrivial dynamics embedded in colored noise: Enhanced Monte Carlo SSA and the case of climate oscillations, *Phys. Lett. A*, 1998, vol. 248, no. 2, pp. 191–202.
- Paluš, M. and Novotna, D., Enhanced Monte Carlo singular system analysis and detection of period 7.8 years oscillatory modes in the monthly NAO index and temperature records, *Nonlinear Processes Geophys.*, 2004, vol. 11, nos. 5–6, pp. 721–729.
- Perminov, V.I. and Pertsev, N.N., Seasonal and nighttime behaviors of emissions of hydroxyl and the atmospheric system of molecular oxygen of the midlatitude mesopause, *Geomagn. Aeron. (Engl. Transl.)*, 2010, vol. 50, no. 4, pp. 518–525.
- Perminov, V.I., Shefov, N.N., and Semenov, A.I., Empirical model of variations in the emission of the molecular oxygen atmospheric system. I. Intensity, *Geomagn. Aeron. (Engl. Transl.)*, 2007, vol. 47, no. 1, pp. 104–108.
- Perminov, V.I., Semenov, A.I., Medvedeva, I.V., and Pertsev, N.N., Temperature variations in the mesopause region according to the hydroxyl-emission observations at midlatitudes, *Geomagn. Aeron. (Engl. Transl.)*, 2014a, vol. 54, no. 2, pp. 230–239.
- Perminov, V.I., Semenov, A.I., Medvedeva, I.V., and Zhelezov, Yu.A., Variability of mesopause temperature from the hydroxyl airglow observations over mid-latitude sites, Zvenigorod and Tory, Russia, *Adv. Space Res.*, 2014b, vol. 54, no. 12, pp. 2511–2517.
- Pertsev, N. and Perminov, V., Response of the mesopause airglow to solar activity inferred from measurements at Zvenigorod, Russia, *Ann. Geophys.*, 2008, vol. 26, no. 5, pp. 1049–1056.
- Plaut, G., Ghil, M., and Vautard, R., Interannual and interdecadal variability in 335 years of central England temperature, *Science*, 1995, vol. 268, pp. 710–713.
- Popov, A.A., Gavrilov, N.M., Perminov, V.I., Pertsev, N.N., and Medvedeva, I.V., Long-term changes in the meso-scale variations of hydroxyl rotational temperature near the mesopause at Tory and Zvenigorod, *J. Atmos. Sol.-Terr. Phys.*, 2020, vol. 205, id 105311. <https://doi.org/10.1016/j.jastp.2020.105311>
- Reid, I.M., Spargo, A.J., and Woithe, J.M., Seasonal variations of the nighttime O(1S) and OH(8-3) airglow intensity at Adelaide, Australia, *J. Geophys. Res: Atmos.*, 2014, vol. 119, pp. 6991–7013.
- Reisin, E.R., Scheer, J., Dyrland, M.E., et al., Traveling planetary wave activity from mesopause region airglow temperatures determined by the network for the detection of mesospheric change (NDMC), *J. Atmos. Sol.-Terr. Phys.*, 2014, vol. 119, pp. 71–82.
- Scargle, J.D., Studies in astronomical time series analysis. II. Statistical aspects of spectral analysis of unevenly spaced data, *Astrophys. J.*, 1982, vol. 263, pp. 835–853.
- Scheer, J., Reisin, E.R., and Mandrini, C.H., Solar activity signatures in mesopause region temperatures and atomic oxygen related airglow brightness at El Leoncito, Argentina, *J. Atmos. Sol.-Terr. Phys.*, 2005, vol. 67, pp. 145–154.
- Semenov, A.I., Bakanas, V.V., Perminov, V.I., Zhelezov, Yu.A., and Khomich, V.Yu., The near infrared spectrum of the emission of the nighttime upper atmosphere of the Earth, *Geomagn. Aeron. (Engl. Transl.)*, 2002, vol. 42, no. 3, pp. 390–397.
- Shefov, N.N., Hydroxyl emission of the upper atmosphere – I. The behavior during a solar cycle, seasons and geomagnetic disturbances, *Planet. Space Sci.*, 1969, vol. 17, pp. 797–813.
- Shefov, N.N., Semenov, A.I., and Khomich, V.Yu., *Izlučenje verkhnei atmosfery — indikator ee struktury i dinamiki* (Upper Atmospheric Radiation: An Indicator of Its Structure and Dynamics), Moscow: GEOS, 2006.
- Sonnemann, G.R., Hartogh, P., Berger, U., and Grygalashvily, M., Hydroxyl layer: Trend of number density and intra-annual variability, *Ann. Geophys.*, 2015, vol. 33, no. 6, pp. 749–767.
- Teiser, G. and von Savigny, C., Variability of OH(3-1) and OH(6-2) emission altitude and volume emission rate from 2003 to 2011, *J. Atmos. Sol.-Terr. Phys.*, 2017, vol. 161, pp. 28–42.
- Wiens, R.H. and Weill, G., Diurnal, annual and solar cycle variations of hydroxyl and sodium nightglow intensities in the Europe–Africa sector, *Planet. Space Sci.*, 1973, vol. 21, pp. 1011–1027.

Translated by V. Arutyunyan